Available online at www.sciencedirect.com
SCIENCE DIRECT®
Biomaterials 25 (2004) 3593–3601
Biomaterials
www.elsevier.com/locate/biomaterials

Biomaterials with hierarchically defined micro- and nanoscale structure

Jian Tan[a,*], W. Mark Saltzman[a,b]

[a] School of Chemical and Biomolecular Engineering, Cornell University, 120 Olin Hall Cornell University, Ithaca, NY 14853, USA
[b] Department of Chemical Engineering, Yale University, New Haven, CT 06511, USA

Received 17 July 2003; accepted 9 October 2003

Abstract

Biomaterials and tissue engineering are becoming increasingly important in biomedical practice, particularly as the population ages. It is clear that cellular responses to materials depend on structural properties of the material at both the micrometer- and nanometer scale, but general methods for controlling material properties on both of these scales are lacking. Using a hierarchical approach that mimics natural material formation processes, we developed a method to produce materials with controlled physical structures at both the micrometer- and nanometer scale. Our method is based upon a pre-organized micropatterned template and conformal transformation of the architecture with nanostructured minerals, namely hydroxyapatite. The newly developed materials were biocompatible with bone cells, induced a range of desirable cellular responses, and may therefore have direct application in bone tissue engineering. In addition, the design principles employed in this study can be extrapolated to the other classes of biomedical materials, including polymers, metals, ceramics or hybrid combinations.

Keywords: Biomineralization; Biomimetic materials; Microstructure; Nanostructure; Bone tissue engineering; Hydroxyapatite; Osteoblast

1. Introduction

Biomaterials offer enormous promise for the repair of lost tissue function [1–3]. The physical structure of a biomaterial is now known to be a key factor that determines cellular responses and hence the range of biomedical applications suitable for a material. Both micrometer [4–7] and nanometer [7–10] scale features of a material significantly influence cell behaviors—such as morphology, migration, adhesion, proliferation and differentiation in vitro and in vivo. As a result, materials with either micron- or nanometer-scale features have been explored in an attempt to improve their performance and have met certain success [5,7,8,10]. It is now apparent that materials that are organized on multiple length scales bear a closer resemblance to biological matrices than those with single scale features, and that materials with multi-scale organization should be more advantageous in biomedical applications. Previous studies demonstrated the ability to make highly ordered materials that ranged from nanoscale silica with laminated, spherical or cylindrical shape organized to microscale hexagons or honeycombs to patterned colloidal nanotopographies [11–14]. However, synthesis of organized structures for direct biomedical applications, with features that can be controlled on both micrometer and nanometer length scales, has not been reported.

We were interested in producing biomaterials for bone regeneration with complex structures in which features of different length scales can be hierarchically organized. To accomplish this objective, we mimicked natural material formation processes. Nature has presented us numerous clues on how to produce complex, organized structures [15–19]. For examples, mineralized tissues, such as bone, teeth and seashells, are usually formed at ambient temperature and in aqueous solutions. The dimension of individual crystallites is usually within the nanometer to micrometer range [16], and yet these fine scale structures are integrated into

*Corresponding author. Tel.: +1-607-255-0559; fax: +1-607-255-9166.
E-mail address: jt75@cornell.edu (J. Tan).

0142-9612/$ - see front matter © 2003 Published by Elsevier Ltd.
doi:10.1016/j.biomaterials.2003.10.034

macroscopic forms with exquisite properties [20]. Although the mechanism of natural biomineralization is not fully understood, many studies suggest that biomineralization is a programmed, stepwise process [16,21]. The process generally starts with the secretion of an organic template by living cells, which proceeds to nucleation and crystal growth steps. In the case of calcium phosphates and calcium carbonates, two extensively studied biological minerals, the chemical composition of the template often consists of insoluble matrix proteins, which forms a micrometer-scale structure, that are decorated with acidic moieties. The insoluble matrix may provide an architectural guide for mineralization and determine the macroscopic form [16,21]; however, the nucleation and crystal growth processes are probably regulated by the exposed acidic groups on the matrix [22,23]. Thus, the key to ordered structure in a biological system could involve hierarchical construction, with separate steps for first building the foundation and then transcription of a finer-scale pattern.

The formation of an organic template in vivo involves complicated cellular processes and is difficult to duplicate in vitro; therefore, we identified an alternative approach. Microfabrication technology, widely used in the semiconductor industry for making electronic materials, offers an excellent tool for building micrometer scale structures [24]. Through computer-aided design and pattern transfer, microfabrication allows the production of pre-defined architectures on a variety of substrates with precisely controlled feature size, shape and spatial distribution [25]. In our hierarchical fabrication method (Fig. 1), micrometer scale architecture was created by microfabrication technology; nanostructured hydroxyapatite (HAP) minerals were then synthesized onto the preset structure using natural mineralization approaches. Since nanostructured HAP is regarded as the major component of bone minerals, the formation of such material may have direct application in bone implantation and tissue engineering. In this study, we demonstrated the biomedical potential of the newly engineered materials.

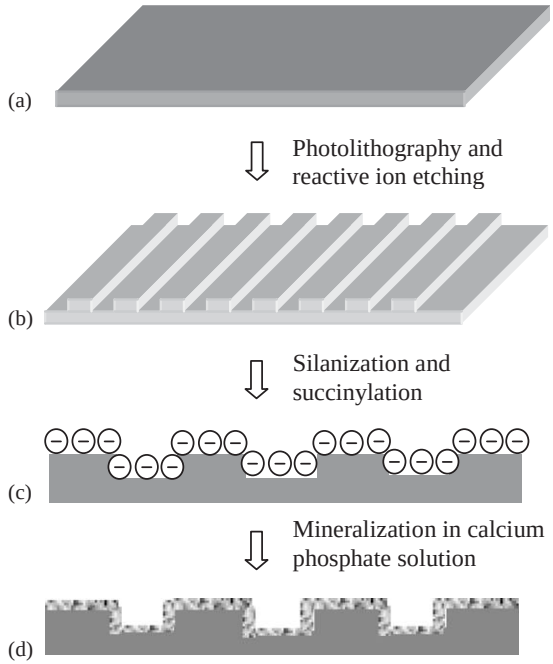

Fig. 1. Schematics of the steps for producing micro- and nanostructured materials: (a) A clean silicon wafer; (b) micrometer scale structures were created using photolithography and reactive ion etching techniques, top view; (c) surface modification, side view. Please note that features were not drawn to scale. Acidic moieties ($-COO^-$) were generated on the surface through silanization and succinylation; (d) a layer of nanostructured calcium phosphate was formed on the patterned surface in supersaturated calcium phosphate solution.

2. Materials and methods

2.1. Fabrication of hierarchically defined micro- and nanoscale structure

The schematic drawing of the fabrication steps is shown in Fig. 1. First, micropatterns were created on silicon wafers at the Cornell Nanofabrication Facility using photolithography and reactive ion etching techniques. Briefly, patterns were designed in CAD and generated in a chrome mask. Photoresist Shipley 1813 was spin-coated onto silicon wafers and exposed through the mask in a GCA 6300 DSW Projection Mask Aligner, $5\times$ g-line stepper. After development in alkaline solutions, exposed photoresist was washed off leaving patches of patterns on silicon wafers. The wafers were dry-etched in a PlasmaTherm SLR-770 ICP Etcher using Bosch™ process. The remaining photoresist was stripped off with acetone and further cleaned in Branson/P2000 barrel etcher.

Second, nanostructured HAP was synthesized on silicon microstructures. The procedure included surface modification with acidic moieties and mineralization in supersaturated calcium phosphate solutions. Surface modification of patterned silicon was achieved by two well-characterized reactions: silanization and succinylation. First, amine groups were attached to silicon patterns through reaction with 3% of (aminopropyl)-triethoxysilane solution for about 10 min [26]. Then, the amine-terminated silicon substrate was immersed in a concentrated (0.1 M) solution of succinic anhydride in anhydrous dimethylformamide (DMF) for 30 min, yielding a carboxyl-terminated surface [27]. Contact angle measurement was performed to verify the reactions [28,29].

Supersaturated calcium phosphate solutions were prepared by dissolving the following ingredients in

de-ionized water: $CaCl_2$, KH_2PO_4, NaCl, KCl, $NaHCO_3$ and Tris-HCl. The pH of the solutions was adjusted and maintained at 7.40 and antibiotics (1% of penicillin and streptomycin from Life Technologies, Grand Island, NY) were added to prevent bacterial growth. The solutions were filtered through 0.2 μm membrane before use. Silicon chips with carboxyl-terminated patterns were immersed in the solutions in a polystyrene plate at 37°C in a moisturized oven. The rate of mineralization was followed every 2 h by: (1) inspecting the solutions and chips in the plate using light microscopy for possible precipitation and (2) if mineralization occurred, the chips were then removed for further examination as described below. In addition, the solutions were refreshed every 24 h to ensure enough ion supplies for mineralization over long period.

2.2. Characterization of engineered materials (AFM, SEM, EDX, XRD)

Silicon chips were removed from the calcium phosphate solutions at various time point for characterization. The samples were rinsed with de-ionized water and blow-dried with air. Micron-scale structure was viewed using scanning electron microscopy (SEM, Leica 440) after coating with a thin layer of Au-Pd (standard SEM sample preparation). Nanoscale structures were examined by both SEM and atomic force spectroscope using tapping mode (AFM, Digital Instruments 3100). Grain size of the particles was measured by AFM analysis. Chemical composition of the minerals was obtained using energy dispersive X-ray analysis (EDX, Jeol 8900 Electron Microprobe). Crystalline phases of the minerals were determined using thin-film X-ray diffraction analysis (XRD, Bruker-Axis general area diffraction detection system).

2.3. Biocompatibility of engineered structures

2.3.1. Cells and culture conditions

Human osteoblast-like Saos-2 and MG-63 cell lines (both from American Type Culture Collection (ATCC), Manassas, VA) were grown in tissue culture (TC) flasks at 37°C in a humidified incubator with 5% CO_2. Saos-2 cells were cultured in McCoy's 5a medium (ATCC) supplemented with 15% of fetal bovine serum (FBS, Life Technologies, Grand Island, NY) and 1% of penicillin and streptomycin (P/S, Life Technologies, Grand Island, NY). MG-63 cells were cultured in Eagle's Minimal Essential medium (MEME, ATCC) supplemented with 10% of FBS and 1% of P/S. Osteogenic supplements (dexamethasone 10^{-8} M, ascorbic acid 50 μg/ml and β-glycerophosphate 10 mM, all from Sigma) were added into the complete growth medium upon cell plating for studies of alkaline phosphatase activity (ALP) of Saos-2 cells.

2.3.2. Morphology

Saos-2 and MG-63 cell lines were cultured at a density of 2×10^4 cells/cm^2 on the micro-, nano-engineered substrates which were cut into about 0.5 cm^2 squares and placed in 24-well TC plates. After 2 days, cells were labeled with fluorescent probes following the experimental protocol from the product information sheet (Molecular Probes, CellTracker Green CMFDA, C-2925). Cells were viewed using fluorescence microscope (Olympus BX-50) and digitized images were acquired using MetaMorph Imaging System (Universal Imaging, Downingtown, PA). In addition, cells were fixed, dehydrated and dried for SEM examination. Briefly, cells were rinsed with phosphate-buffer saline solution (PBS) three times before being fixed in 4% of formaldehyde/PBS solution for 15 min. Then they were rinsed with PBS and dehydrated with a series of graded ethanol solutions. The samples were dried in a critical point drier (EM 850, Fort Washington, PA) and sputter coated with Au–Pd immediately after for best preservation of the structures.

2.3.3. Adhesion

The measurement of Saos-2 cells adhesion was performed 4 h after the cells were plated onto various substrate at a density of 2×10^4 cells/cm^2. All the samples were placed in a humidified incubator with 5% CO_2 at 37°C. Cells were rinsed with PBS twice and the adherent cells were dislodged from the substrates with Trypsin-EDTA. The cells were collected and the numbers were determined using the CellTiter 96 AQ_{ueous} One Solution Cell Proliferation Assay (MTS assay, Promega).

2.3.4. Proliferation

The proliferation of cells on various surfaces was determined by the measurement of live cells on the substrates at 3 days of culture using MTS assay as described above.

2.3.5. Alkaline phosphatase activity (ALP)

ALP was measured using a commercially available kit (104-LL, Sigma). Briefly, cells were lysed using the M-PER Mammalian Protein Extraction Reagent (Pierce) after 3 days of culture. The cell lysates were collected and the ALP activity was determined using the reaction of *p*-nitrophenol conversion to *p*-nitrophenylate at 37°C for 15 min. The ALP activity was normalized by the total intracellular protein synthesis as measured by BCA assay (Pierce).

Each of the adhesion, proliferation and ALP activity experiments was repeated at least three times in quadruplicates. Statistical analyses were performed using the two-tailed *t*-test assuming equal variance for two samples.

3. Results and discussion

We first patterned parallel ridges/channels (R/C) (Fig. 2a) as a framework to guide the spatial organization of nanostructured HAP. This pattern was selected because it was expected to have immediate visible effect on cell morphology and orientation, enabling determination of its biological impact [5]. Other patterns, such as pillars, can be easily generated depending on particular applications (Fig. 2b). Silicon was chosen as a starting material because it is the most widely used material in microfabrication. However, the design principle defined in Fig. 1 can be applied to other materials of biological relevance with minor technical modification (such as pattern generation and surface chemical reaction, details of which depend on the materials). In fact, we have already used this approach to mineralize polystyrene surfaces and patterned hydrogels (unpublished data).

We expected that anionic groups on the template would play an active role in the control of nucleation and crystal growth during the biomineralization phase of structure formation [30–33]. Therefore, we attached –COOH groups to the surfaces using silanization and succinylation (Fig. 1c). After silanization, the advancing water contact angle of silicon surfaces increased to 55° from 40° for surfaces without any chemical modification; it became 48° after the exposure of COOH groups through succinylation [28,29].

After chemical modification, micropatterned materials were immersed in supersaturated calcium phosphate solutions for mineral deposition for up to 3 days (Fig. 1d). As a control experiment, silicon surfaces without any chemical modification were subjected to the mineralization step. We found that mineralization could be induced under certain conditions (e.g. high supersaturation or long induction period), but the size of crystals was large (~1 μm) and the resulting mineral layer was not continuous. Based on a series of studies, we determined that chemical modification of the foundation layer was essential to achieve control over subsequent nanoscaled structure formation.

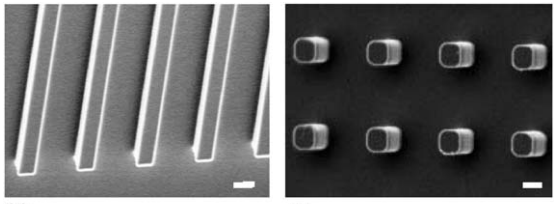

Fig. 2. SEM images of microscale structures. (a) Parallel ridges/channels patterned on silicon substrate. The width and height of the ridges are 4 μm and spacing is 10 μm. (b) Regular arrays of pillars (4 × 4 × 4 μm) patterned on silicon substrate. Scale bars represent 4 μm.

We found that the rate and pattern formation of nanostructured HAP on the micropatterned surfaces strongly depended on solution conditions. The initial selection of solutions was based upon body fluids and cell culture medium composition, as we expected that minerals formed under these conditions would be stable in culture and in the body (Table 1 and Fig. 3). In solution A (the highest thermodynamic driving force), homogeneous nucleation easily occurred within 6 h, resulting no minerals or few on silicon chips. Homogenous precipitation could also result in the formation of undesirable crystalline phases, such as dicalcium phosphate dihydrate (DCPD) and octaclacium phosphate (OCP) (Fig. 3). In solution B, heterogeneous nucleation occurred within 8 h; the morphology of minerals was thin-plate like after 24 h and the mineral layer was nearly continuous and continued growth for up to 72 h. In solution C, heterogeneous nucleation occurred within 24 h; the minerals eventually became thin-plate like, however, the growth rate was slow and it stopped growing after 48 h. In solution D, crystallization did not occur within 24 h. We determined the proper solutions for nanostructured HAP formation using the following criteria: (1) chemical composition, (2) phase and structure, (3) morphology, (4) the rate of mineralization and (5) the quality of the mineral layer. Therefore, solution B was used in the experiments hereafter.

The resulting mineralized structures were examined by SEM at various times after initiation of mineralization. SEM images indicated that nucleation and crystal growth appeared on the patterned substrate within 8 h (Fig. 4a). The initial precipitates were round and distinct. After 24 h, a nearly continuous layer of minerals was formed on the patterned surface (Fig. 4b),

Table 1
Solution parameters for the synthesis of hydroxyapatite at 37°C

Solution	Ca (mM)	P (mM)	Mineral formation
A	3.8	1.5	Spontaneous precipitation
B	2.5	1.0	Continuous film of nano-scale HAP
C	1.0	0.6	Discontinuous film of HAP
D	0.6	0.3	No mineral formation

In addition to Ca and P listed, the solutions consisted of KCl (4 mM), $NaHCO_3$ (4.2 mM), NaCl (1.44 M) and Tris-HCl (0.05 M).

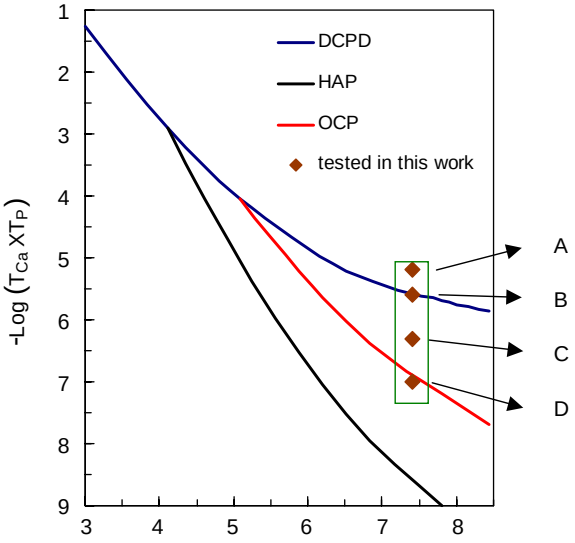

Fig. 3. Phase diagram of calcium of phosphate solutions at 37°C and ionic strength 0.15 mol/l, the logarithm of the product of total calcium and phosphate concentrations is plotted as a function of solution pH. The tendency for a calcium phosphate phase to precipitate in solution could be assessed from this diagram. Most biological fluids fall into the box in the plot. A number of solutions (A, B, C and D) within physiological range were tested in order to obtain uniform nanostructured HAP layer on the patterned substrate. In solution A, homogeneous nucleation occurred; in solution B, heterogeneous nucleation of HAP occurred on silicon chips and continuous film of HAP formed; in solution C, heterogeneous nucleation of HAP occurred on silicon chips but no continuous film of HAP formed and in solution D, no mineralization. Solution B was selected for the experiments hereafter. DCPD, dicalcium phosphate dihydrate; HAP, hydroxyapatite and OCP, octacalcium phosphate.

and the mineral morphology changed to thin and plate-like. As the reaction continued past 24 h, the appearance of minerals remained the same while the patterned ridges became evidently wider (Fig. 4c). Similar results were obtained for the mineral formation on pillared structures (Fig. 4d). Close examination of the mineral revealed nanometer-scale texture with thin plates of less than 100 nm on the patterned surface (Fig. 4e). The mean size of the minerals was 56 ± 32 nm as determined by AFM, the size did not change to any significant degree with reaction time up to 3 days (Fig. 4f). Thin-film XRD of the minerals revealed a polycrystalline structure without any preferred orientation with regard to the substrate (indicated by the uniform arch of the spectrum, Fig. 5a). The diffraction pattern, with characteristic broad HAP peaks (Fig. 5b), was similar to that of bone minerals [34]. There was a slight increase in intensity, but not sharpness (Fig. 5b), with reaction time reflecting the increase in the amount of crystallites. Chemical analysis of energy dispersive X-ray spectrum (Fig. 5c) indicated the molar Ca/P ratio of the minerals was 1.63 ± 0.04, close to that of bone (which averages at 1.70 [34]). Together, these results suggest that we produced nanostructured HAP on a microstructured template with crystal properties similar to those of bone minerals.

It should be noted that the thickness of mineral layer can be arbitrarily selected and precisely controlled, while the crystal structure and morphology are maintained. The thickness (d) of the mineral layer was calculated from the width of ridges ($d = 1/2(W_t - W_0)$, where W_0 and W_t are the width of the silicon ridge before and after

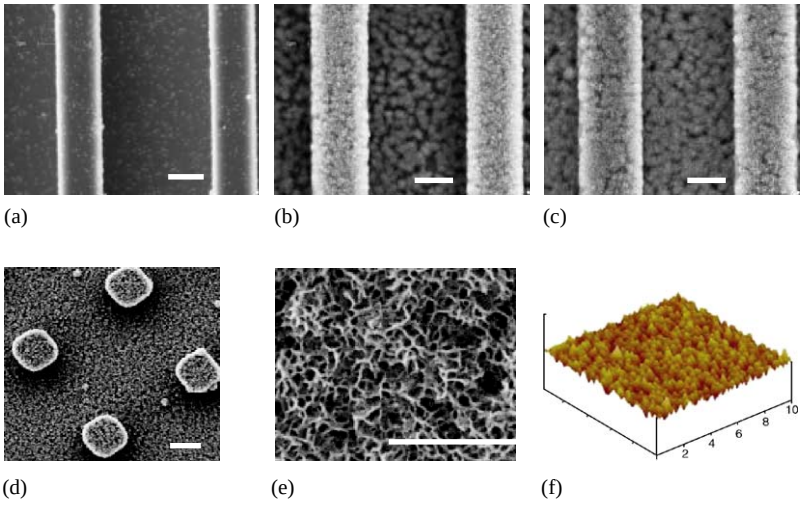

Fig. 4. SEM images of micro- and nanoscale structures. (a) After 8 h in supersaturated calcium phosphate solution, discrete and round initial crystallites were formed on the patterned substrate. (b) After 24 h, the crystallites became thin-plate like and started to form a continuous layer on the patterned substrate. The width of the ridges was 5.1 μm. (c) After 48 h, the morphology of crystals remained the same while the mineral layer became more uniform and continuous. The width was increased further to 5.7 μm. (d) Nanostructured HAP was organized into pillared structural form. (e) High magnification image of minerals shows a clear thin-plate structure with the plate thickness at ~100 nm. Scale bars on SEM images represent 4 μm. (f) AFM images of minerals, the average grain size was determined at 56 ± 32 nm, in agreement with the SEM study.

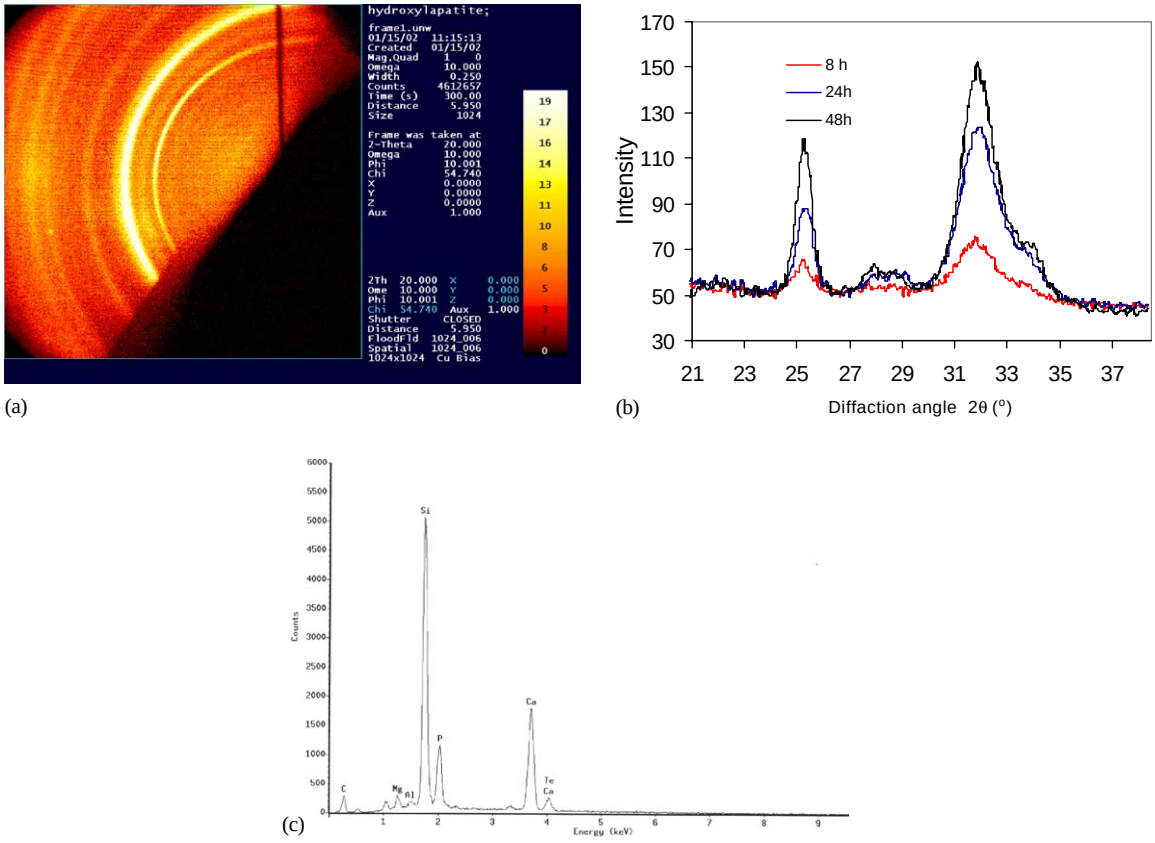

Fig. 5. (a) Typical thin-film X-ray diffraction pattern of the mineral layer on patterned silicon substrate. The uniform arches indicated that the crystals were polycrystalline with random orientation. (b) Integration of a selected range of the area in the pattern yielded the intensity pattern as a function of diffraction angle. The peaks, although broad, are characteristic of HAP. The peaks remained broad after 48 h but the intensity was enhanced due to the increase in the amount of crystallites. (c) Energy dispersive X-ray spectrum of the mineral layer at 8 kev. The electrons were able to penetrate the HAP layer, so silicon was also detected. Quantitative chemical analysis indicated that the molar Ca/P ratio was 1.63 ± 0.04.

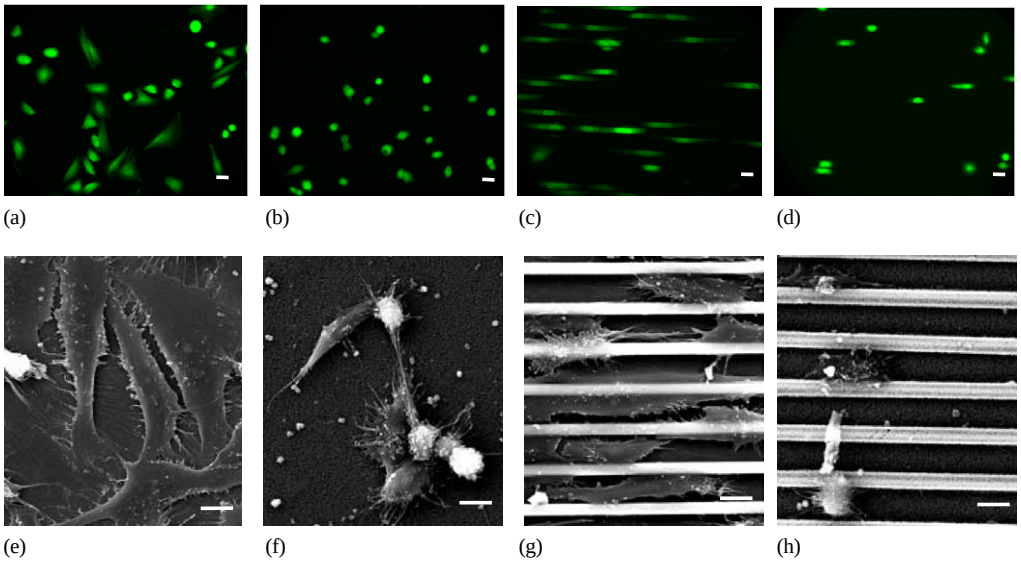

Fig. 6. Biocompatibility studies of human osteoblast-like cells (Saos-2) cultured on various surfaces. Fluorescent light microscopic (a–d) and SEM (e–h) images of Saos-2 cells on smooth silicon (S) surface (a and e), nanostructured (N) surface (b and f), microstructured (M) surface (c and g) and micro/nanoengineered (MN) surface with parallel ridges (d and h). Cells are rounded on N surfaces (b and f) as compared to cells on S surfaces (a and e). Cells were apparently oriented on M and MN surfaces with parallel ridges (c,d,g,h). All scale bars represent 10 μm.

mineralization). After the initial induction period, the mineral layer reached about 800 nm in thickness in about 48 h. This is a reasonable growth rate that allows us to control film thickness with nanometer precision. From the design point of view, the change in feature size due to the addition of a mineral layer can be compensated for within the microscale pattern created during lithography. Compared to tissue engineering scaffold structures that are made of polymer network [6,35], this hierarchical approach provides precise preservation of dimension in the final structure, both on micro- and nanoscale, which we expect to be important in controlling cellular behavior.

To examine cellular interactions with these materials, we cultured human osteoblast-like cells, Saos-2 and MG-63, on various micro- and nanostructured surfaces. Silicon surfaces without any structures (smooth surface, S), with micrometer scale features only (micropatterned, M) or with nanometer scale features only (biomineralized, N) were compared to surfaces formed with the full hierarchical approach (micro/nanostructured, MN). Cell morphology on surfaces with micropatterned parallel ridges/channels (R/C, Fig. 4) were used because we expected the ridges to restrict the cell shape, which is known to influence growth, differentiation and phenotypical expression of cells significantly [36]. Both cell lines on micro (M), nano (N) and micro/nano (MN) structured surfaces showed markedly different morphologies. Shown in Fig. 6a–h, Saos-2 cells were less spread and more rounded on N and MN surfaces (Figs. 6b,d,f and h) than on S and M surfaces (Figs. 6a,c,e and g). Because both N and MN surfaces were coated with HA while S and M were not, we believe that the rounded cell shape probably reflects the influence of nanoscale surface structure on cell spreading. Furthermore, the cells on M and MN surfaces aligned along the direction of ridges (Figs. 6c,d,g and h), but not on S and N surfaces (Figs. 6a,b,e and f). We believe that such preferred cell orientation reflects the influence of the microscale structure in producing "contact guidance", which can control the direction and speed of cell migration [37,38]. Similar results were obtained for MG-63 cells. It should be noted that the morphology of cells on MN and N materials was most similar to that observed in the in vivo microenvironment; previous studies have suggested that such morphology is essential to ex vivo bone formation [39].

To further explore the function of cells on hierarchically prepared materials, the adhesion, proliferation and function of cells were measured for cells cultured on surfaces patterned with pillars (Figs. 2e and 4d). No significant differences in Saos-2 cell adhesion were observed between S, M, N or MN materials, although adhesion to all was about 50% less than TC surfaces which are optimized to support cell adhesion (Fig. 7a). The rate of cell proliferation on S, M, and N surfaces, determined after 3 days of culture, was comparable to TC polystyrene, while cell proliferation on the MN surface was about 40% less (Fig. 7a). Notably, however, ALP, which is used to characterized early osteoblastic differentiation [40], was significantly greater for Saos-2 cells on MN surfaces compared to untreated silicon surfaces and was similar to TC surfaces (Fig. 7b),

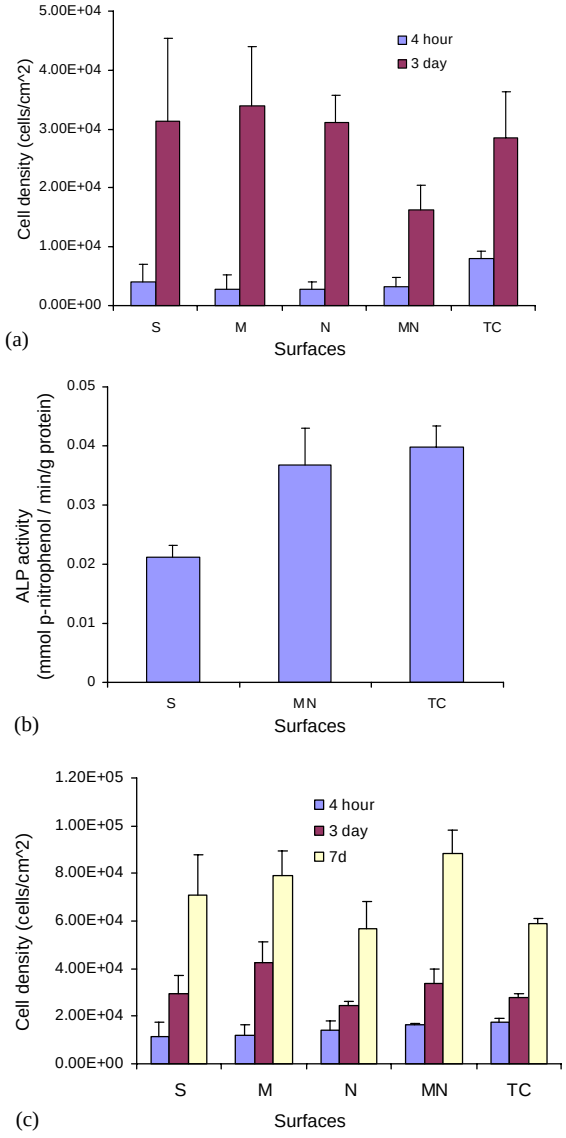

Fig. 7. Cell adhesion and proliferation studies on micro/nanostructured (MN), microstructured only (M), nanostructured only (N), untreated silicon surface (S) or tissue culture surface (TC). (a) Saos-2 cells on pillared surfaces. Cells adhesion was significantly greater on TC surface than all other surfaces. The rate of proliferation was similar on M, N, S and TC surfaces, but significantly less on MN surface ($P<0.03$). (b) ALP activity of Saos-2 cells on MN materials was significantly greater than S surface ($P<0.01$) and was similar to tissue culture (TC) surface. (c) MG-63 cells on pillared surfaces. There was not any significant difference in adhesion between MN, M, N, S and TC surfaces after 4 h. The rate of proliferation was greater on MN and M surfaces than N, S and TC surfaces after 3 days of culture and it was the greatest on MN surface after 7 days of culture ($P<0.03$).

Table 2
Summary of biocompatibility studies of various surfaces using Saos-2 cells

Cell behavior	Substrate				
	Smooth	Micro	Nano	Micro/nano	Tissue culture
Shape[a]	Flat	Flat	Round-up	Round-up	Flat
Orientation[a]	Random	Parallel to the ridge	Random	Parallel to the ridge	Random
Adhesion[b]	=	=	=	=	+
Proliferation[b]	=	=	=	–	=
ALP activity[b]	=	+	+	+	+

Note: The microstructure of "a" was parallel ridges/channels and "b" was pillars. The adhesion, proliferation and ALP activity on micro/nano, micro, nano or tissue culture plate was compared to smooth silicon surface (+, – or =).

indicating that the hierarchically prepared surfaces supported osteoblast function. Interestingly, while the adhesion of MG-63 cells (a different class of human osteoblast-like cell line) on MN surface was similar to TC surface, the rate of proliferation on MN surface was greatest among all the surfaces (Fig. 7c). Because ALP activity was very low for MG-63 cells, the result was not analyzed in this study. Taken together (Table 2, Figs. 6 and 7), these results indicate that the MN surfaces are biocompatible and support the growth and function of cultured cells. We believe that these materials provide a good in vitro system for studying cell behavior and a potential scaffold material for tissue engineering.

4. Conclusion

We have produced a novel biomaterial using strategies inspired by natural mineralization process. This material has a complex structural form in which a nanometer scale mineral phase is organized in a controlled fashion on a micrometer scale template that is preset by a controllable microfabrication process. One advantage of this approach is that it allows precise control of material structures on both micrometer and nanometer length scale. The ability to control material structure with this precision will enable us to program desirable and predictable cellular responses into a three-dimensional biomaterials. Our study suggests a potential future for hierarchical synthesis of materials for biomedical applications.

Acknowledgements

The authors thank Profs. A. Vignery and M. Zeichner-David for reading the manuscript and providing helpful suggestions, Ms. M. Ma and T. Watkins for technical assistance. This work was supported by a grant from NIH (DE-14097). It was performed in part at the Cornell Nano-Scale Facility which is supported by NSF under the grant ECS-9319005 and the Cornell Center for Materials Research which is supported by NSF under the Grant DMR-9632275.

References

[1] Peppas NA, Langer R. New challenges in biomaterials. Science 1994;263:1715–9.
[2] Griffith LG. Emerging design principles in biomaterials and scaffolds for tissue engineering. Ann NY Acad Sci 2002;961:83–95.
[3] Hench LL, Polak JM. Third-generation biomedical materials. Science 2002;295:1014–7.
[4] Ito Y. Surface micropatterning to regulate cell functions. Biomaterials 1999;20:2333–42.
[5] Brunette DM, Chehroudi B. The effects of the surface topography of micromachined titanium substrata on cell behavior in vitro and in vivo. J Biomech Eng 1999;121(1):49–57.
[6] Tan J, Shen H, Saltzman WM. Micron-scale positioning of features influences the rate of polymorphonuclear leukocyte migration. Biophys J 2001;81:2569–79.
[7] Wilkinson CDW, et al. The use of materials patterned on a nano- and micro-metric scale in cellular engineering. Mater Sci Eng C 2002;19:263–9.
[8] Curtis A, Wilkinson C. Topographical control of cells. Biomaterials 1997;18(24):1573–83.
[9] Rajnicek AM, Britland S, McCaig CD. Contact guidance of CNS neurites on grooved quartz: influence of groove dimensions, neuronal age and cell type. J Cell Sci 1997;110:2905–13.
[10] Webster TJ, et al. Enhanced functions of osteoblasts on nanophase ceramics. Biomaterials 2000;21:1803–10.
[11] Sellinger A, et al. Continuous self-assembly of organic–inorganic nanocomposite coatings that mimic nature. Nature 1998;394:256–60.
[12] Cha JN, et al. Biomimetic synthesis of ordered silica structures mediated by block copolypeptides. Nature 2000;403:289–92.
[13] Dan N. Synthesis of hierarchical materials. TIBTECH 2000;18:370–4.
[14] Wood MA, Riehle M, Wilkinson CDW. Patterning colloidal nanotopographies. Nanotechnology 2002;13:605–9.
[15] Heuer AH, et al. Innovative materials processing strategies: a biomimetic approach. Science 1992;255(5048):1098–105.
[16] Lowenstam HA, Weiner S. On biomineralization. New York: Oxford Press; 1989.
[17] Mann S. Biomineralization and biomimetic materials chemistry. J Mater Chem 1995;5:935–46.
[18] Stupp SI, Braun PV. Molecular manipulation of microstructures: biomaterials, ceramics, and semiconductors. Science 1997;277:1242–8.

[19] Morse DE. Silicon biotechnolgy: harnessing biological silica production to construct new materials. TIBTECH 1999;17:230–2.
[20] Mann S, Ozin GA. Synthesis of inorganic materials with complex form. Nature 1996;382:313–8.
[21] Mann S, Webb J, Williams RJP. Biomineralization: chemical and biochemical perspectives. New York: VCH; 1989.
[22] Addadi L, Weiner S. Interactions between acidic proteins and crystals: stereochemical requirements in biomineralization. Proc Natl Acad Sci 1985;82:4110–4.
[23] Belcher AM, et al. Control of crystal phase switching and orientation by soluble mollusc-shell proteins. Nature 1996;381:56–8.
[24] Hoch HC, Jelinski LW, Craighead HG, editors. Nanofabrication and biosystems. New York: Cambridge University Press; 1996.
[25] Madou M. Fundamentals of microfabrication. New York: CRC Press; 1996.
[26] Tai H, Buettner HM. Neurite outgrowth and growth cone morphology on micropatterned surfaces. Biotech Prog 1998;14:364–70.
[27] Chance JJ, Purdy WC. Fabrication of carboxylic acid-terminated thin films using polyethyleneimine on a gold surface. Langmuir 1997;13:4487–9.
[28] Simon A, et al. Study of two grafting methods for obtaining a 3-aminopropyltriethoxysilane monolayer on silica surface. J Colloid Interface Sci 2002;251:278–83.
[29] Liu Q, et al. The role of surface functional groups in calcium phosphate nucleation on titanium foil: a self-assembled monolayer technique. Biomaterials 2002;23:3103–11.
[30] Bunker BC, et al. Ceramic thin-film formation on functionalized interfaces through biomimetic processing. Science 1994;264:48–54.
[31] Tanahashi M, Matsuda T. Surface functional group dependence on apatite formation on self-assembled monolayers in a simulated body fluid. J Biomed Mater Res 1997;34:305–15.
[32] Aizenberg J, Black AJ, Whitesides GM. Control of crystal nucleation by patterned self-assembled monolayers. Nature 1999;398:495–8.
[33] Murphy WL, Mooney DJ. Bioinspired growth of crystalline carbonate apatite on biodegradable polymer substrate. J Am Chem Soc 2002;124(9):1910–7.
[34] LeGeros RZ. Calcium phosphate in oral biology and medicine. Basel, Switzerland: Karger; 1991.
[35] Kim B, Mooney DJ. Development of biocompatible synthetic extracellular matrices for tissue engineering. TIBTECH 1998; 16:224–30.
[36] Chen CS, et al. Geometric control of cell life and death. Science 1997;276:1425–8.
[37] Fishman RB, Hatten ME. Multiple receptor systems promote CNS neural migration. J Neuro Sci 1993;13(8):3485–95.
[38] Tan J, Saltzman WM. Topographical control of human neutrophil motility on micropatterned materials with various surface chemistry. Biomaterials 2002;23:3215–25.
[39] Kale S, et al. Three-dimensional cellular development is essential for ex vivo formation of human bone. Nature Biotech 2000; 18:954–8.
[40] Bancroft GN, et al. Fluid flow increases mineralized matrix deposition in 3D perfusion culture of marrow stromal osteoblasts in a dose-dependent manner. Proc Natl Acad Sci USA 2002; 99:12600–5.